fibers

Article

A New *Fabric Reinforced Geopolymer Mortar* (FRGM) with Mechanical and Energy Benefits

Fabio Longo [1], Alessio Cascardi [2],*, Paola Lassandro [2] and **Maria Antonietta Aiello [1],[2]**

[1] Department of Innovation Engineering, University of Salento, 73100 Lecce, Italy; fabio.longo@unisalento.it (F.L.); antonietta.aiello@unisalento.it (M.A.A.)

[2] ITC-CNR, Construction Technologies Institute—Italian National Research Council, 70124 Bari, Italy; paola.lassandro@itc.cnr.it

* Correspondence: alessio.cascardi@itc.cnr.it

check for updates

Abstract: A large part of the European building Heritage is dated back over centuries. Consequently, its structural and thermal performances are often inadequate. Commonly, different interventions are proposed for solving these issues separately. However, reasonable drawbacks arise when the structural retrofitting requires a direct contact with the target-member while the insulation layer is potentially interposed in between. In this scenario, the present research proposes a novel and unique system able to guarantee both the energetic and the structural retrofitting. *Inorganic Matrix Composites* (IMCs) are a promising solution in this sense. Among them, the *Fabric Reinforced Cementitous Matrix* (FRCM) is one of the most used; or rather a composite made of a fabric (open grid or mesh) within an inorganic matrix (lime or cement based). Even if the inorganic matrix has a relevant thickness (if compared with the one of the fabric), its thermal resistance is insufficient. The novelty of this work consists in assessing a new geo-polymeric FRCM-system by combining fly-ash binder (reused material) and expanded glass aggregate (recycled material). Direct tensile tests, for measuring the tensile strength, ultimate strain and elastic modulus, were performed in addition to thermal conductivity tests. The results were compared with those of traditional FRCM (commercially available). The potentiality of the proposal for structural and energy retrofitting is discussed and examples of its possible application are also reported.

Keywords: FRCM; integrated design; sustainable building renovation; thermo-mechanical analysis; combined seismic and energy retrofits; new material

1. Introduction

The safety level and the thermal insulation capacity stated in current standard and technical codes often do not meet the actual mechanical and thermal properties of existing buildings, [1–3]. For this reason, the interest in retrofitting systems for structural and energetic purposes is steadily increasing [4]. This study focused on the use of *Inorganic Matrix Composite* (ICM), or more specifically on the *Fabric Reinforced Cementitious Mortar* (FRCM), which is a composite made up of a fiber mesh (or grid) bounded on a structural member by means of an inorganic matrix, [5–11]. In the recent past, a combined solution was studied by considering the *side-by-side* installation of FRCM and thermal insulation layers in order to achieve both the seismic and the thermal improvements of infill [5]. Even if the efficiency of the proposal was found relevant, the methodology requires two separate designs, on-site time-consuming operations and a significant cost. However, the ICM-system is potentially able to improve simultaneously the mechanical and thermal performances of the buildings. In fact, the fabric is a high-strength material while the matrix has a relevant thickness, which may lead to a significant thermal-resistant layer.

As well known in literature, the tensile constitutive law of a FRCM can be approximated to a bi-linear curve where the first and the second slope are dominated respectively by the properties of the matrix and the fabric, [12]. In some cases, an intermediate slope was also found to be corresponding to the cracking phase of the matrix and, at the same time, the slippage of the fabric within it. Generally, this phase is not significant (in term of strain and stiffness) when compared with the other two. Recent studies proved that the matrix plays a key-role in affecting the mechanical performances of the FRCM-system in terms of strength and ductility [12–18].

In literature, numerous contributions can be found in the field of FRCM characterization referring to the mechanical point of view. The first challenge when dealing with FRCM was computing the tensile characteristic behavior. Different testing methods and specimen preparation were tested in many laboratories in order to reach a standard test procedure. The *gripping method* is now recognized in European countries. Available technical codes (e.g., in the Italian CNR DT 215, [19]) consider the tensile stress-strain law to be tri-linear depending of the level of damage of the matrix. Hence, the third branch (used for design purpose) assumes a slope almost equal to the elastic modulus of the dry fabric in tension. The scientific literature reports on a significant number of tests on FRCMs exhibiting often a bi-linear approximation.

Three different textiles within the cementitious matrix were investigated in [20]; such as steel, carbon and basalt textile. From tensile tests, it was observed that the steel-FRCM shows a somewhat higher strength before tensile failure and better bonding between the textile and matrix when compared to the carbon-FRCM and basalt-FRCM.

In many cases, FRCM specimens were exposed to a particular environmental condition in order to evaluate the durability and the curing effect [19–24]. The specimens were found sensitive to the curing temperature, exposition and relative humidity mainly depending on the properties of the matrix. Furthermore, different systems were tested and compared, by varying both the type of fabric or matrix, [25–29]. The results confirmed the direct influence of the matrix and the fabric regarding respectively the first and the second slope of the tensile law (when bi-linear), respectively. In recent years, some geopolymer-based matrices were tested demonstrating valuable efficiency due to the high level of compressive strength of the matrix [30,31]. Based on authors' knowledge, the potential thermal application of FRCM (and particularly when geopolymer-based) was never investigated.

From the thermal point of view, the effectiveness of retrofitting essentially depends on two-parameters: the thickness and the conductivity. In FRCMs, the thickness of the matrix is relevant (i.e., 10–30 mm per side in case of single layer application), but the thermal conductivity is not insulating-oriented. Alternatively, an inorganic matrix can be associated with pre-impregnated fabric. In this case, a *Composite Reinforced Mortar* (CRM) is obtained and a mortar thickness greater than 30 mm is accomplished [32]. Thus, CRMs are even more relevant in the perspective of a novel insulating-oriented matrix; while structural strengthening capacity is well demonstrated in the literature [33–36].

Usually, insulating plaster (without mechanical strengthening scope) is effectively adopted for energy retrofitting in a sandwich-like assessment (e.g., expanded cork/infill/ventilated wall/finishing), [37]. On the other hand, the application to a substrate of both the insulating plastering and the strengthening system compromises the bond between each other and consequently the mechanical effectiveness of the strengthening. Alternatively, the addition of *Light-Weight Aggregate* (LWA) into the plastering was examined in the recent past [38]. However, it was found that it may improve the thermal capacity (depending on the volumetric ratio) while dramatically decreasing the mechanical strength making it useless for the scope.

For this reason, a new ICM system, herein called *Fabric Reinforced Geopolymer Matrix* (FRGM) was assessed by using fly ash, metakaolin and expanded glass aggregate. This type of material is promising, since it exhibited good mechanical properties and lower thermal conductivities with respect to standard structural materials [39,40]; the mortar mix was aimed to obtain comparable mechanical strength, compared to traditionally mortars used for FRCMs, but a significantly lower thermal conductivity.

Available results in terms of mechanical and energetic performance were used to assess an optimal mix-design of the proposed geopolymer mortar [41]. In such a way a relevant innovation was provided by this research, in fact, no other materials with comparable double-performances are currently available. Finally, two series of glass-IMC (with traditional and innovative matrix) were tested in direct tension and then compared.

2. Materials and Methods

This section is focused on the description of the used materials and the test methods for the physical and the mechanical characterization.

2.1. Materials and Sample Preparation

The traditional FRCM was made of a *Natural Hydraulic Lime* (NHL) mortar; which was supplied as a dry powder pack to be mixed with 17% by weight (wt) of tap water. The dry pre-mix consists of hydraulic lime, sand and chemical admixtures according to the commercially available technical sheet. The *Geopolymer Matrix* (GPM) was made of dry binders (fly ash and metakaolin), alkali activators and LWA (i.e., expanded glass aggregate). The chemical composition and the density of the dry constituents are both reported in Table 1. The chemical composition was measured by means of XRF for fly ash, while data concerning both the metakaolin and the LWA were declared by the supplier. The preparation of the alkali activator solution was made at least 24 h before mixing all constituents. In detail, it was performed by mixing *Sodium Silicate* (SS) and *Sodium Hydroxide* (SH) into distilled water with SS/SH weight ratio set equal to 2.5. Later on, the alkali solution was mixed (low speed) with the dry binders. Finally, the LWA was added into the alkali-activated binder. The GPM was assessed according to [42]. The weight percent mix-proportions of the obtained NHL and GPM is reported in Figure 1a,b, respectively.

Table 1. Chemical composition of fly ash and metakaolin.

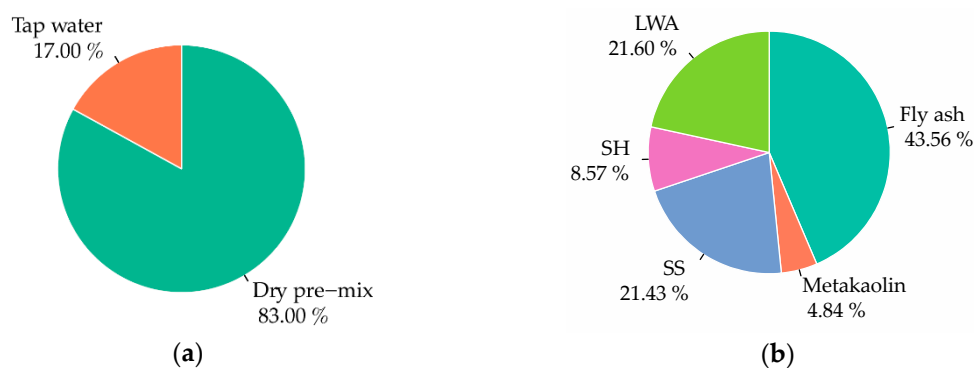| Component	Oxide Concentration %								Particle Density g/cm^3
	SiO$_2$	CaO	Na$_2$O	Al$_2$O$_3$	Fe$_2$O$_3$	K$_2$O	TiO$_2$	SO$_3$	
Fly ash	37.33	6.13	-	16.14	30.79	5.28	3.65	0.68	2.30
Metakaolin	55.00	0.30	-	40.00	1.40	0.80	1.50	-	2.40
LWA	72.50	9.00	13.00	3.25	-	2.25	-	-	0.57

Figure 1. Percentage by weight of the constituents: (**a**) *Natural Hydraulic Lime* (NHL); (**b**) *Geopolymer Matrix* (GPM).

The experimental program involved both tests on the matrix and the FRCM. At this scope, two series of specimens were prepared: NHL- and GPM-based. The same fabric was used for FRCM system, i.e., an *Alkaline-Resistant* (AR) glass fiber arranged as 12 × 12 mm^2 mesh (40 mm^2/m equivalent thickness) with 1400 MPa, 2% and 74 GPa as tensile strength, maximum elongation and *Young's modulus*,

respectively (according to the manufacturer technical sheet). As suggested by technical Guidelines [43], a total of 9 FRCM samples was tested per series. The coupons, sized $600 \times 60 \times 10$ mm^3 in order to include at least four longitudinal yarns of fabric, were cast in a single polystyrene formwork and cured for 28 days at environmental temperature and *Relative Humidity* (i.e., ~23 ± 2 °C and ~50 ± 5% RH). After curing, steel tabs ($80 \times 60 \times 2$ mm^3) were epoxy-glued at the specimen ends on both sides.

2.2. Test Methods

The dry mass' density of the mortar specimens was measured by weighing three cylinders of 35 mm in diameter and 55 mm in height per series. The thermal conductivity was measured against the same oven-dried specimens by the *Modified Transient Plane Source* (MTPS) technique (TCA Thermal Conductivity Analyzer, C-Therm), according to ASTM standard [44]. The contact surface of the transducer was polished with sand paper, in order to minimize surface roughness, and then cleaned with pressurized air. Furthermore, the contact between the transducer and the sample was ensured by placing a film of thermal paste in addition to a weight (500 g) above the sample. The performance of the device was preliminarily checked by measuring a series of control materials (with standard known property) as suggested by the provider and the results were found reliable.

Two triplets (i.e., NHL and GPM) of $40 \times 40 \times 160$ mm^3 prisms were prepared and tested with 3-points bending set (span equal to 100 mm). When the flexural failure occurred, the prisms were divided in two and the resulting parts were tested in compression by considering $40 \times 40 \times 40$ mm^3 samples according to UNI EN 1015-11 [45]. Furthermore, the *Young's modulus* of the mortars was herein evaluated by computing the secant slope between 5% and 33% of the peak stress in compression. FRCM-specimens were tested in direct tensile stress-state and displacement control (Figure 2a,b for FRCM and FRGM, respectively). The test velocity was set equal to 0.2 mm/min according to [43]. A 100-kN load cell was assigned to the load recording; while deformations were measured with a clip-on extensometer. The latter was equipped with knife edges, positioned at the gage length (=10 cm), in direct contact with the specimens (see Figure 2c). Moreover, a camera was placed in front of the plan view of the specimen in order to video record the crack's development during the test.
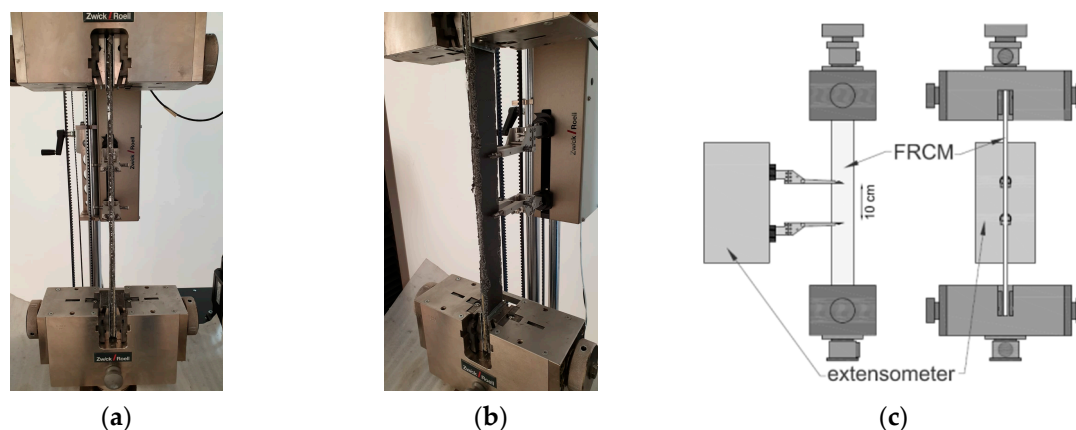

(**a**)　　　　　　　(**b**)　　　　　　　(**c**)

Figure 2. FRCM direct tensile test set-up: (**a**) front view; (**b**) lateral view; (**c**) sketch.

Finally, *Scanning Electron Microscopy* (SEM) was performed using a *Zeiss Scanning Electron Microscope Evo40*, [46]. Small fragments, including the fabric, were extracted from the middle cross-section of the FRCM-coupon after the tensile test. The micrographs at the matrix-fabric interface were acquired at 20 kV accelerating voltages.

3. Results

In the following sections, the results about energy and mechanical performance of the tested materials were reported for comparison. The evaluation aimed to evidence the competitive mechanical

properties of the FRCM with respect to the FRGM. Moreover, the relevant scatter in terms of thermal capacity between the two systems is underlined.

3.1. Energy Performance

The dry mass density (ρ) and the thermal conductivity (λ) significantly change the potential application field of the material. As well known, a lightweight, porous material generally insulates from both the acoustic and the thermal point of view, even if pores ease the crack opening due to loading. In Table 2, the results of the mass density and thermal conductivity measurements were collected, as also shown in Figure 3 for the sake of clarity. In particular, the GPM samples revealed a mass density ~33% lower than the NHL ones. The principal reason of this difference was linked to the use of LWA. In fact, the bulk density was 1500 kg/m^3 and 450 kg/m^3 for the NHL and GPM aggregate, respectively. For this reason, the FRGM is particularly suitable for structural retrofitting because it provides less additional weight with respect to the FRCM. As a consequence, negligible variations of both gravity loads and seismic inertia-like actions affect the strengthened structure.

Table 2. Dry mass density and thermal conductivity of NHL and GPM.

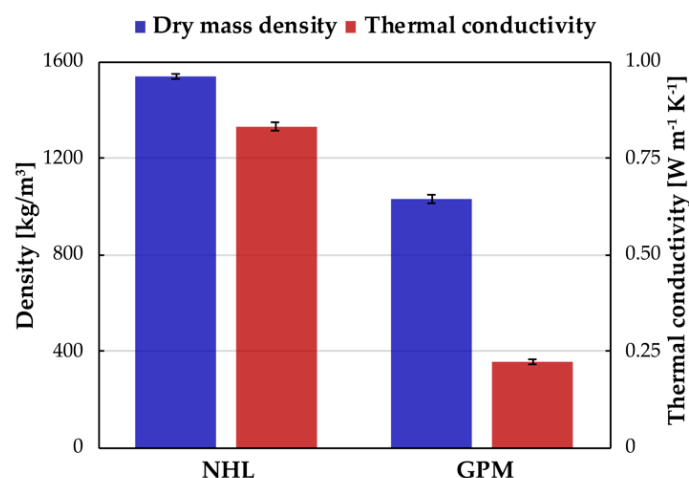| Label	Dry Mass Density (ρ)			Thermal Conductivity (λ)		
	Mean kg/m^3	CoV [1] %	ρ GPM/ρ NHL %	Mean W m^{-1} K^{-1}	CoV [1] %	λGPM/λNHL %
NHL	1540	0.5	66.95	0.830	1.5	26.75
GPM	1031	1.8		0.222	2.7	

[1] Coefficient of Variation.

Figure 3. Dry mass density and thermal conductivity of NHL and GPM.

More relevant was the difference in terms of thermal conductivity. In fact, the GPM exhibited a ~73% lower value if compared with NHL. Again, the LWA's effect was crucial (expanded glass having ~60% porosity). Even the binder (i.e., alkali-activated fly ash and metakaolin) is generally less conductive than traditional binders, i.e., lime and cement based [40].

3.2. Mechanical Performance

The mean values of the mortars' mechanical properties were reported in Table 3 and Figure 4 in terms of flexural/bending (f_b) and compressive strength (f_c) and *Young's modulus* (**E**), with the relative dispersions (i.e., CoV). The GPM reached ~6 MPa compressive strength; which was slightly lower than that obtained for the NHL, but adequate for the ICM-application. Depending on the type of fly ash, the compressive strength of the GPM could be improved as measured in on-going research by the same

authors. Generally, NHL matrix exhibited higher mechanical performances, especially in terms of stiffness. Nonetheless, according to the available literature, the proposed GPM has proper characteristics for being involved in FRCM systems, even if a lower initial elastic stiffness of FRCMs is expected.

Table 3. Flexural strength, compressive strength and *Young's modulus* of NHL and GPM.

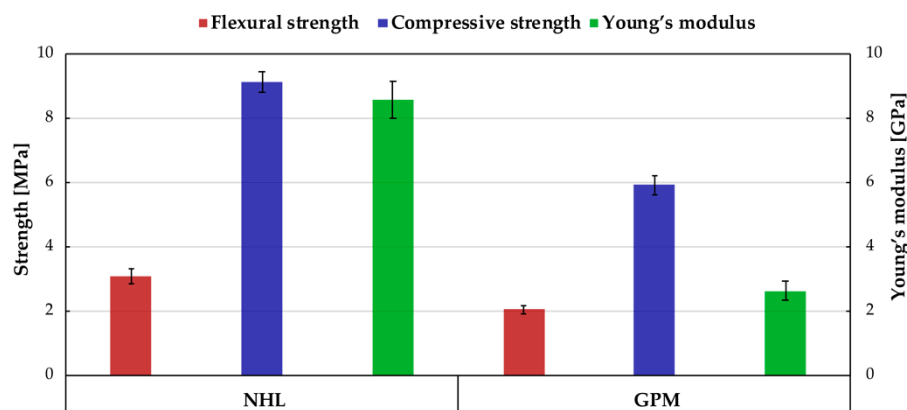| Label | Flexural Strength (f_b) | | | Compressive Strength (f_c) | | | Young's Modulus (E) | | |
	Mean MPa	CoV [1] %	$f_{b,GPM}/f_{b,NHL}$ %	Mean MPa	CoV [1] %	$f_{c,GPM}/f_{c,NHL}$ %	Mean GPa	CoV [1] %	E_{GPM}/E_{NHL} %
NHL	3.10	7.4	66.45	9.13	3.3	64.95	8.58	8.9	37.64
GPM	2.06	6.3		5.93	5.0		3.23	10.2	

[1] Coefficient of Variation.

Figure 4. Compressive strength, flexural strength and *Young's modulus* of NHL and GPM.

The stress strain relationships of FRCM and FRGM were reported in Figure 5a,b. In detail, the stress was evaluated dividing the applied load by the cross-section of the fabric, while the strain is related to the gauge length (see Figure 2c). The tensile strength (σ_u) and the ultimate strain (ε_u) are both reported in Table 4, while Table 5 shows the un-cracked (E_I) and cracked slopes (E_{II}) of the ICM-systems. As expected, the initial stiffness (i.e., first phase modulus) is directly affected by the stiffness of the matrix used in the FRCM system. Nonetheless, the dispersion area showed that the global behavior of the system is pretty similar in both cases, Figure 6. The stresses are properly transferred from the matrix to the fabric, as proven by the similar slope of the second phase. All the specimens exhibited a quasi bi-linear behavior and a fabric-rupture failure, generally occurring in the middle-height of the coupon (see Figure 7).
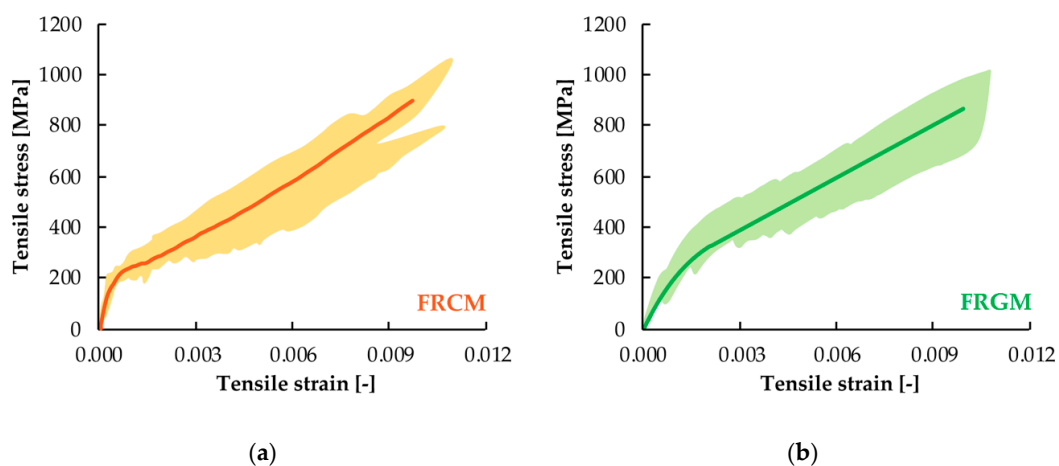

(a)

(b)

Figure 5. Stress strain relationship of FRCM (**a**) and FRGM (**b**).

Table 4. Tensile strength, maximum strain and elastic moduli of FRCM and FRGM.

Label	Tensile Strength (σ_u)			Ultimate Strain (ε_u)		
	Mean MPa	CoV [1] %	$\sigma_{u,GPM}/\sigma_{u,NHL}$ %	Mean %	CoV [1] %	$\varepsilon_{u,GPM}/\varepsilon_{u,NHL}$ %
NHL	890.75	15.7		0.87	19.0	
GPM	867.69	10.7	97.41	0.87	19.4	100.00

[1] Coefficient of Variation.

Table 5. Un-cracked slope and cracked slope of FRCM and FRGM.

Label	Un-Cracked Slope [2] (E_I)			Un-Cracked Slope [3] (E^*_I)			Cracked Slope (E_{II})		
	Mean GPa	CoV [1] %	$E_{I,GPM}/E_{I,NHL}$ %	Mean GPa	CoV [1] %	$E^*_{I,GPM}/E^*_{I,NHL}$ %	Mean GPa	CoV [1] %	$E_{II,GPM}/E_{II,NHL}$ %
NHL	514.47	8.5		2.52	8.3		77.45	5.1	
GPM	229.33	9.8	44.59	1.12	9.8	44.59	69.13	5.4	89.26

[1] Coefficient of Variation; [2] Computed according to the fabric cross-section = 2.4 mm^2; [3] Computed according to the matrix cross-section = 600 mm^2.
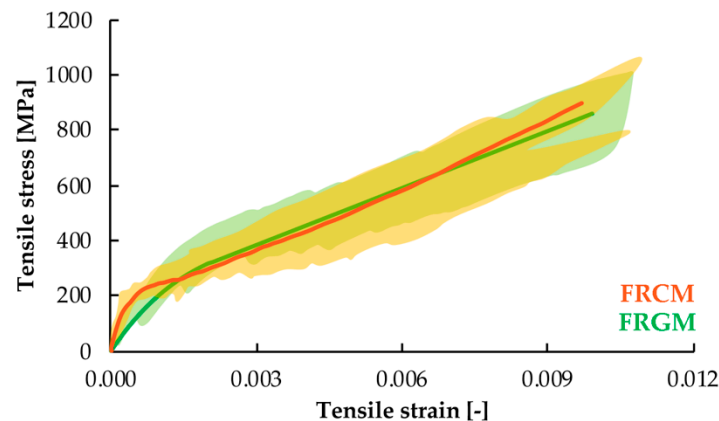

Figure 6. FRCM and FRGM stress strain relationships overlapping.

Finally, the SEM micrographs in Figure 8 were taken to make an estimation the short-term effects of the geopolymer binder on AR-glass fabric. In other words, the alkaline environment, generated from the reaction of SS and SH with dry binders (fly ash and metakaolin in this case), represents a potential cause of damaging for both LWA and mesh fiber. A chemical corrosion usually leads to surface cracking of the fabric, [47]. In this study, a first step to explore this issue was made, looking at fabric surface after 28 days. Moreover, the surface of glass in the GPM-matrix was compared with the one in the NHL-matrix. In detail, Figure 8a shows the fabric-matrix interface zone of FRCM, while Figure 8b reports a zoom of the surface of the fabric. Because of the low alkalinity of NHL-matrix, the fabric-surface was smooth and no chemical corrosion was found. The matrix-fabric interface zone (Figure 8c) and fabric surface (Figure 8d) were analyzed also for FRGM sample. Again, it was not noticed any remark of chemical corrosion. In this experimental campaign, only short-term effects were considered. Further studies can estimate the chemical and mechanical characteristics of the material after accelerated aging according to [43].
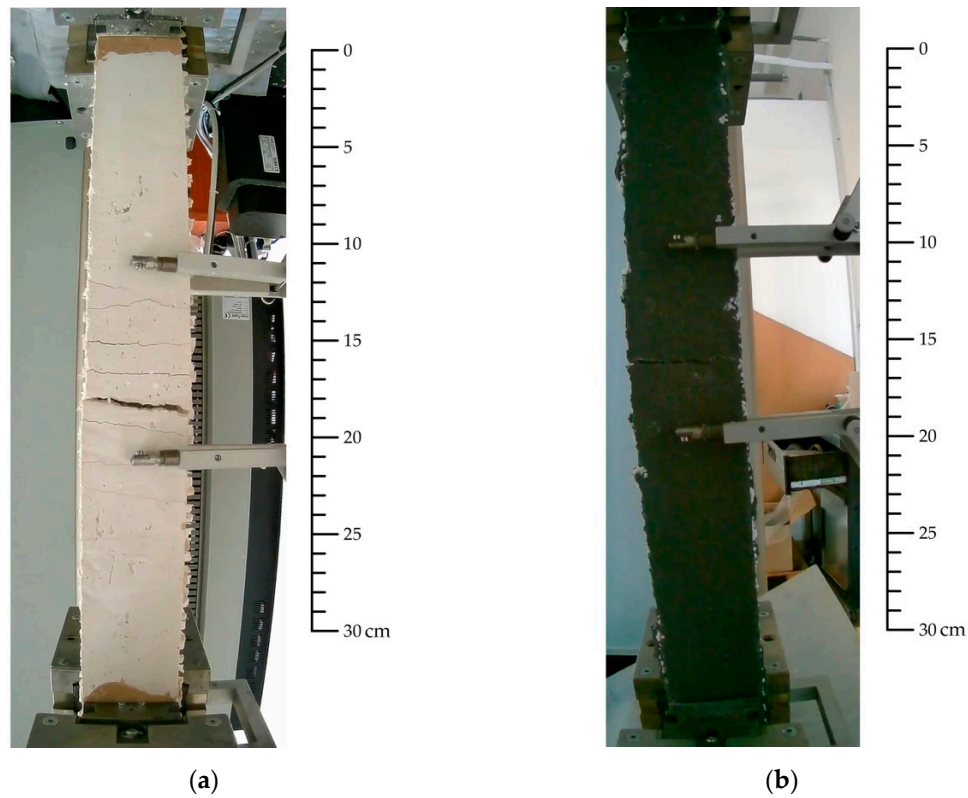
(**a**)　　　　　　　　　　　　　　　　　　　　(**b**)

Figure 7. FRCM-systems crack patterns: NHL (**a**) and GPM (**b**).

(**a**)　　　　　　　　　　　　　　　　　　　　(**b**)

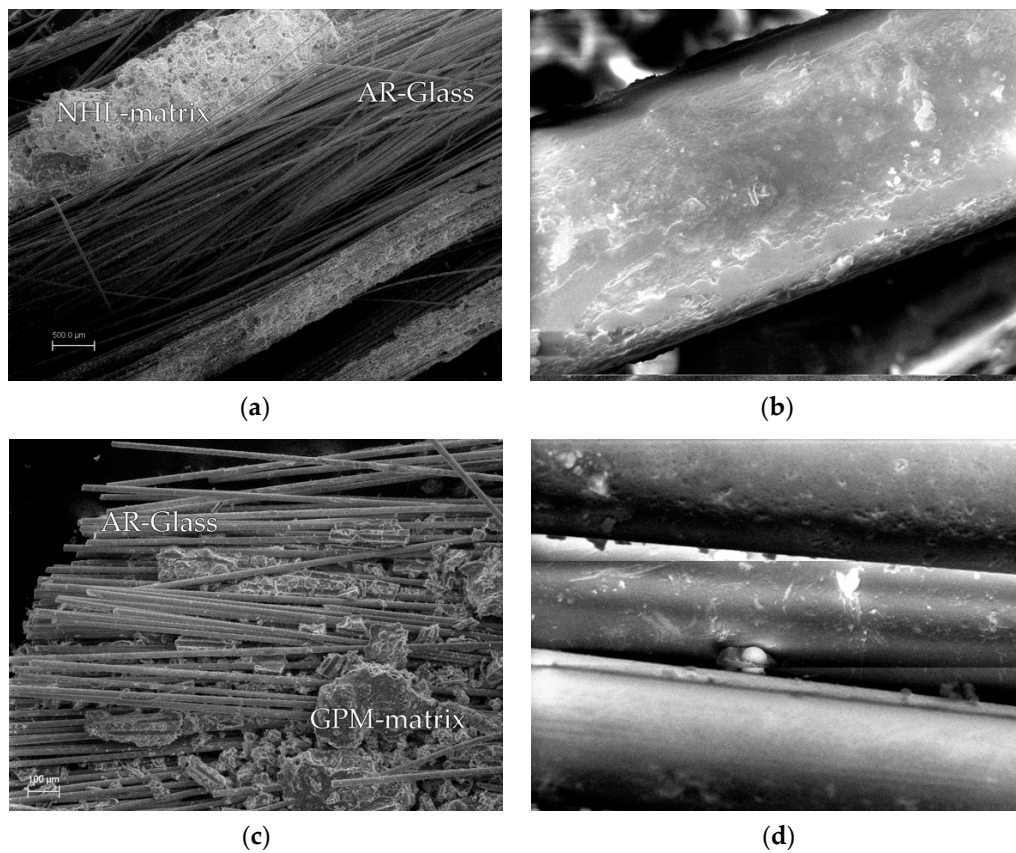(**c**)　　　　　　　　　　　　　　　　　　　　(**d**)

Figure 8. SEM images of AR-Glass fiber within FRCM, (**a**) overview and (**b**) detail, and within FRGM, (**c**) overview and (**d**) detail.

4. Mechanical and Energetic Retrofitting: Applications

The experimental outcomes demonstrated that the mechanical strength of the FRGM system could be compared to the one traditionally made of lime-based mortar (if same fabric is considered); while a significant reduction of the thermal conductivity was obtained. Moreover, the direct tensile tests highlighted that the performances in terms of tensile stress strain behavior were similar. Thus, the proposed FRGM-system is a candidate for a totally novel application as retrofitting system aimed to both energy and mechanical benefits.

In order to check the effectiveness of the system for possible mechanical and energetic retrofitting, some ideal applications were analyzed in the following section. Two masonry walls typically found in existing building context were considered. The former was a $100 \times 100 \times 25$ cm^3 *Solid Clay Brick* (SCB) masonry wall (Figure 9a,b), the latter a *Tuff Brick Masonry* (TBM) wall with the same dimensions (Figure 9c,d). For both of them a poor-resistant lime-based mortar was examined for the bed joints.
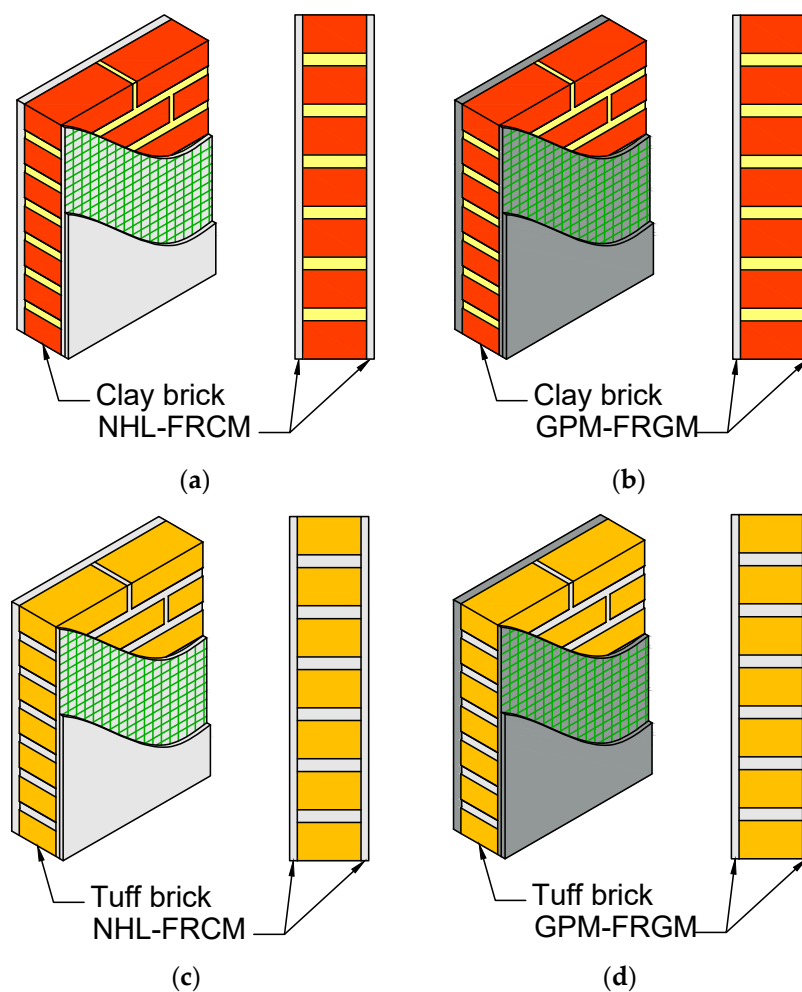

Clay brick
NHL-FRCM

(**a**)

Clay brick
GPM-FRGM

(**b**)

Tuff brick
NHL-FRCM

(**c**)

Tuff brick
GPM-FRGM

(**d**)

Figure 9. Schematic view of (**a**) FRCM- and (**b**) FRGM-system on the clay brick masonry wall and (**c**) FRCM- and (**d**) FRGM-system on the *Tuff* brick masonry wall.

Results obtained by retrofitting the walls using the FRGM system were reported. The shear strength of the reinforced masonry walls V_{eff} was evaluated by the analytical model suggested in [13] and reported in Equations (1)–(8), because it is both matrix and fiber dependent (i.e., V_{mat} and V_f respectively). In fact, the matrix properties (i.e., matrix net area $A_{n,mas}$ and compressive strength f_{mat}) were herein the discriminant which affected the mechanical difference between the two reinforcing systems. Whereas, the properties of the fabric (i.e., fabric net area $A_{n,f}$ and tensile strength f_f) were the

same in both the systems. The mechanical properties of the masonry wall (i.e., f_{mas} and $f_{t,mas}$ or rather the compressive and tensile strength respectively), which are essential to compute the shear strength, were considered according to [48]. Moreover, to evaluate the energetic performance of the four masonry walls, a calculation of thermal transmittance was performed [49]. The thermal conductivity of the unreinforced masonry walls was estimated according to [50,51]. The mechanical and thermal results were collected in Table 6.

Table 6. Shear strength and thermal transmittance of solid clay and *Tuff* brick masonry retrofitted with FRCM and FRGM.

Label	Shear Strength		Thermal Transmittance	
	Unreinforced MPa	Reinforced MPa	Unreinforced W m^{-2} K^{-1}	Reinforced W m^{-2} K^{-1}
SCB – FRCM	0.85	1.07	1.471	1.330
SCB – FRGM	0.85	1.05	1.471	1.053
TBM – FRCM	0.67	0.90	1.258	1.153
TBM – FRGM	0.67	0.88	1.258	0.939

Some interesting remarks can be outlined from the reported results. Despite a matrix with a lower compressive strength, the FRGM system allowed a theoretical shear strength gain very similar to that obtained by using the NHL matrix. In fact, the reinforced/unreinforced shear strength ratios (Figure 10) were equal to 126%, 125%, 133% and 131% for SCB-FRCM, SCB-FRGM, TBM-FRCM and TBM-FRGM, respectively. On the other hand, the thermal transmittance for the considered samples manifested an important gain when involving the GPM-matrix. In the case of SCB, the adoption of the FRGM led to a reduction of heat transfer approximately equal to 29%, while the FRCM reduced it just of 10%. Similarly, if a TBM is considered, the reduction of heat transfers for the case of GPM-matrix and NHL-matrix is about 25% and 9%, respectively.

$$V_{eff} = \alpha f_{mas}^{0.5} \cdot A_{n,mas} + V_f + V_{mat} \tag{1}$$

$$V_f = \frac{2}{3} A_{n,f} \cdot 0.5 f_f \tag{2}$$

$$V_{mat} = 0.1 \cdot A_{n,mat} \cdot f_{mat}^{0.5} \tag{3}$$

$$\alpha = \frac{0.363}{1 + e^{-\nu}} \tag{4}$$

$$\nu = -0.52 + 1.36\beta + 0.05\gamma \tag{5}$$

$$\beta = \frac{f_f \cdot A_{n,f}}{f_{t,mas} \cdot A_{n,mas}} \tag{6}$$

$$f_{t,mas} = 0.7 \sqrt{f_{mas}} \tag{7}$$
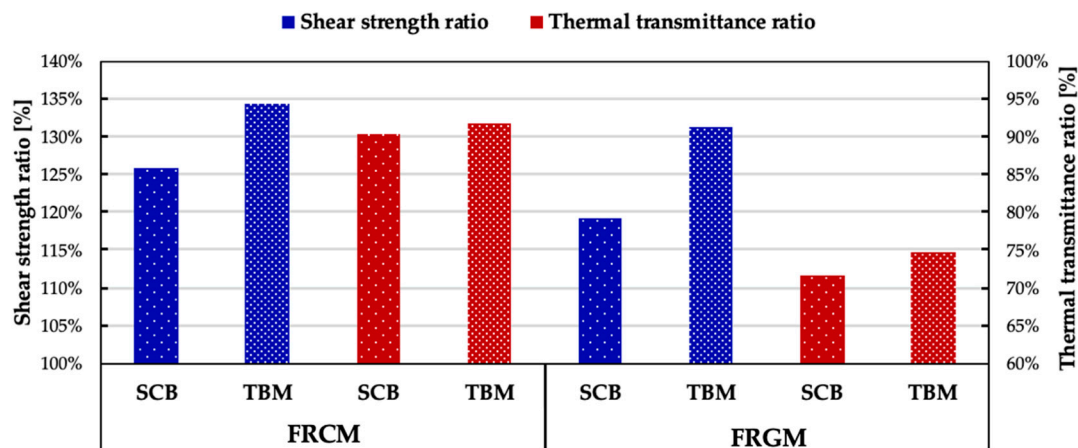
$$\gamma = \frac{f_{mat}}{f_{mas}} \tag{8}$$

Figure 10. Shear strength ratio and Thermal transmittance ratio of SCB and TBM samples with both FRCM- and FRGM-systems, with respect to the unreinforced sample.

Another interesting application that was explored is the retrofitting of horizontal structural elements, as masonry vaults. Generally, the issues of this application are linked to the weight density of the proposed solution and its thermal properties, besides the mechanical performances. The FRGM herein proposed represents a competitive system, which can inhibit the failure mechanism of a vault or an arch (typically linked to a cinematic configuration, rather than to a material failure) without adding a relevant weight and preserving the thermal insulation capacity, or adding more insulating power. An example of thermal simulation was performed by a 2D model of a TBM vault, involving a multi-physics computation tool [52]. The material above the vault is typically a masonry filler (Figure 11a), but it was replaced with an ICM 10 cm layer in Figure 11b to evaluate the difference in thermal conductivity of the horizontal structure. The section of the vault and the filler were modelled using a material with the same thermal properties of the above-defined TBM. The surfaces were inserted in a conductive medium set along the borders with a fixed temperature, 10 °C. The ground has a low thermal conductivity, i.e., 0.001 W m^{-1} K^{-1}, so it behaves as an adiabatic plane. In both figures all the elements were initially set to 10 °C, except the heater, whose surface is fixed at 50 °C. From the initial set until the equilibrium, the heat transfer occurred because of conduction and convection (i.e., solar radiation was neglected in this simulation).
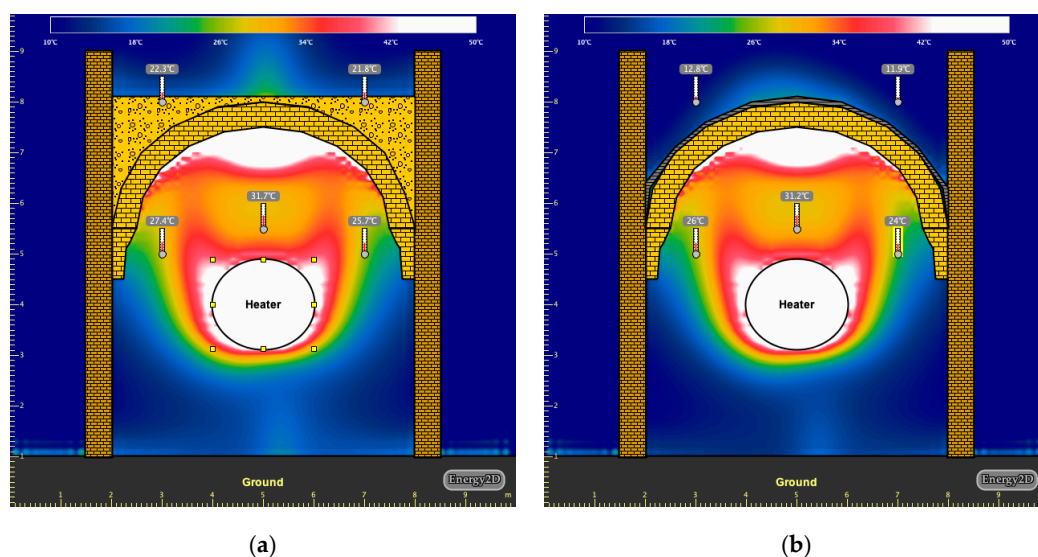

Figure 11. Thermal simulation results of (**a**) a TBM masonry vault and (**b**) the same vault with the infill substituted with a geopolymer-based ICM.

The results referred to the stage corresponding to the thermal equilibrium, i.e., when thermometers did not register any further time-dependent change. The recorded surface's temperatures highlighted that the layer of GPM is more efficient to insulate than the infill usually involved in vaults, despite a much lower thickness. Furthermore, it is well-known that the configuration in Figure 11b is more performant from the mechanical point of view, because of the ICM-strengthening [53].

5. Conclusions

Building heritage is nowadays inadequate with respect to the prescriptions of current technical Codes, particularly referring to the thermal and the mechanical (static or seismic) performances. Generally, practitioners have experience in one of these two fields. Thus, independent retrofitting solutions are commonly accomplished in order to mitigate the energy dispersion or the structural vulnerability; often generating conflicts. The present investigation was aimed to study a unique ICM-based system focused on the thermal and mechanical capacity improvement of buildings. In fact, the fabric was chosen based on the high tensile strength; while the matrix was designed in order to have low thermal conductivity. Fly ash, metakaolin, alkali activators and expanded glass aggregates were combined in a proper proportion (geopolymer) for the scope.

Experimental results are promising and it is the authors' opinion that the proposed material is worthy of further research due to its total innovative nature. In fact, the mechanical properties of FRGM are comparable to traditional FRCM. In particular, the scatter between the two ICMs in terms of ultimate strength and strain is negligible (i.e., <3%), while a lower initial stiffness was recorded for FRGM. These results are consistent with the characterization of FRGM-mortar, which is less resistant and stiff. On the other hand, the FRGM-system exhibited a higher thermal insulation power, which decreased the thermal conductivity of about 25%. Another interesting aspect is related to the mass density of GPM, which is 33% lower than the NHL one. Thus, the magnification of gravity and inertial loads is limited when compared to current market-available solutions. An open issue, related to the long-term behavior of the system is target of further investigations, despite the 28 days SEM analysis was found encouraging.

Finally, some design examples were proposed in the present work, supported by theoretical calculation. The mechanical results highlighted that FRGM is a valid alternative for retrofitting with respect to the FRCM, since the scatter in terms of shear strength gain is lower than 5% (when the same type and amount of fabric are considered). Contrarily, the reduction in thermal transmittance is significant, as the application of FRGM leads to a ~25% reduction instead of ~10% for the FRCM.

Conflicts of Interest: The authors declare no conflict of interest.

References

1. Gkournelos, D.P.; Bournas, D.A.; Triantafillou, T.C. *Combined Seismic and Energy Upgrading of Existing Buildings Using Advanced Materials*; EUR 29172 EN; Publications Office of the European Union: Luxembourg, 2019; ISBN 978-92-79-81824-0. [CrossRef]
2. Ministerial Decree 17 January 2018, NTC 2018. Norme Tecniche per le Costruzioni, Ministero delle Infrastrutture. Available online: http//www.cslp.it (accessed on 30 July 2020). (In Italian)

3. Ministerial Decree 26 June 2015. In *Applicazione Delle Metodologie di Calcolo Delle Prestazioni Energetiche e Definizione Delle Prescrizioni e dei Requisiti Minimi Degli Edifici*; n. 162, 15-07-2015—Suppl. Ordinario n. 39; Gazzetta Ufficiale: Rome, Italy, 2015.

4. Artino, A.; Evola, G.; Margani, G.; Marino, E.M. Seismic and Energy Retrofit of Apartment Buildings through Autoclaved Aerated Concrete (AAC) Blocks Infill Walls. *Sustainability* **2019**, *11*, 3939. [CrossRef]

5. Pohoryles, D.A.; Maduta, C.; Bournas, D.A.; Kouris, L.A. Energy Performance of Existing Residential Buildings in Europe: A Novel Approach Combining Energy with Seismic Retrofitting. *Energy Build.* **2020**, *223*, 110024. [CrossRef]

6. Ombres, L.; Iorfida, A.; Mazzuca, S.; Verre, S. Bond analysis of thermally conditioned FRCM-masonry joints. *Measurement* **2018**, *125*, 509–515. [CrossRef]

7. Ombres, L.; Mancuso, N.; Mazzuca, S.; Verre, S. Bond between Carbon Fabric-Reinforced Cementitious Matrix and Masonry Substrate. *J. Mater. Civ. Eng.* **2018**, *31*, 4018356. [CrossRef]

8. Pekmezci, B.Y.; Arabaci, E.; Ustundag, C. Freeze-Thaw Durability of Lime Based FRCM Systems for Strengthening Historical Masonry. *Key Eng. Mater.* **2019**, *817*, 174–181. [CrossRef]

9. Tilocca, A.R.; Incerti, A.; Bellini, A.; Savoia, M. Influence of Matrix Properties on FRCM-CRM Strengthening Systems. *Key Eng. Mater.* **2019**, *817*, 478–485. [CrossRef]

10. Castellano, A.; Fraddosio, A.; Scacco, J.; Milani, G.; Piccioni, M.D. Dynamic Response of FRCM Reinforced Masonry Arches. *Key Eng. Mater.* **2019**, *817*, 285–292. [CrossRef]

11. Ombres, L.; Verre, S. Flexural Strengthening of RC Beams with Steel-Reinforced Grout: Experimental and Numerical Investigation. *J. Compos. Constr.* **2019**, *23*, 4019035. [CrossRef]

12. Cascardi, A.; Micelli, F.; Aiello, M.A. FRCM-confined masonry columns: Experimental investigation on the effect of the inorganic matrix properties. *Constr. Build. Mater.* **2018**, *186*, 811–825. [CrossRef]

13. Cascardi, A.; Micelli, F.; Aiello, M.A. Analytical model based on artificial neural network for masonry shear walls strengthened with FRM systems. *Compos. Part B Eng.* **2016**, *95*, 252–263. [CrossRef]

14. Cascardi, A.; Longo, F.; Micelli, F.; Aiello, M.A. Compressive strength of confined column with Fiber Reinforced Mortar (FRM): New design-oriented-models. *Constr. Build. Mater.* **2017**, *156*, 387–401. [CrossRef]

15. Cascardi, A.; Aiello, M.A.; Triantafillou, T. Analysis-oriented model for concrete and masonry confined with fiber reinforced mortar. *Mater. Struct.* **2017**, *50*, 202. [CrossRef]

16. Faella, C.; Napoli, A.; Realfonzo, R. Confinement of Concrete with FRCM Materials. In *Proceedings of Italian Concrete Days 2018*; Di Prisco, M., Menegotto, M., Eds.; Springer: Cham, Switzerland, 2018.

17. Thermou, G.E.; Hajirasouliha, I. Compressive behaviour of concrete columns confined with steel-reinforced grout jackets. *Compos. B Eng.* **2018**, *138*, 222–231. [CrossRef]

18. Minafò, G.; La Mendola, L. Experimental investigation on the effect of mortar grade on the compressive behaviour of FRCM confined masonry columns. *Compos. Part B Eng.* **2018**, *146*, 1–12. [CrossRef]

19. CNR—Advisory Committee on Technical Recommendations for Construction. *Guide for the Design and Construction of Externally Bonded Fibre Reinforced Inorganic Matrix Systems for Strengthening Existing Structures*; CNR: Rome, Italy, 2019.

20. Wang, X.; Lam, C.C.; Iu, V.P. Comparison of different types of TRM composites for strengthening masonry panels. *Constr. Build. Mater.* **2019**, *219*, 184–194. [CrossRef]

21. Ombres, L. Analysis of the bond between fabric reinforced cementitious mortar (FRCM) strengthening systems and concrete. *Compos. Part B Eng.* **2015**, *69*, 418–426. [CrossRef]

22. Nobili, A.; Signorini, C. On the effect of curing time and environmental exposure on impregnated Carbon Fabric Reinforced Cementitious Matrix (CFRCM) composite with design considerations. *Compos. Part B Eng.* **2017**, *112*, 300–313. [CrossRef]

23. Wang, X.; Lam, C.C.; Sun, B.C.; Noguchi, T.; Iu, V.P. Effect of curing environment on the tensile behaviour of FRCM composites. *Constr. Build. Mater.* **2020**, *238*, 117729. [CrossRef]

24. Butler, M.; Mechtcherine, V.; Hempel, S. Durability of textile reinforced concrete made with AR glass fibre: Effect of the matrix composition. *Mater. Struct.* **2010**, *43*, 1351–1368. [CrossRef]

25. Ascione, L.; de Felice, G.; De Santis, S. A qualification method for externally bonded Fibre Reinforced Cementitious Matrix (FRCM) strengthening systems. *Compos. Part B Eng.* **2015**, *78*, 497–506. [CrossRef]

26. Donnini, J.; Corinaldesi, V.; Nanni, A. Mechanical properties of FRCM using carbon fabrics with different coating treatments. *Compos. Part B Eng.* **2016**, *88*, 220–228. [CrossRef]

27. D'Antino, T.; Papanicolaou, C. Mechanical characterization of textile reinforced inorganic-matrix composites. *Compos. Part B Eng.* **2017**, *127*, 78–91. [CrossRef]
28. Donnini, J.; Corinaldesi, V. Mechanical characterization of different FRCM systems for structural reinforcement. *Compos. Part B Eng.* **2017**, *145*, 565–575. [CrossRef]
29. De Carvalho Bello, C.B.; Boem, I.; Cecchi, A.; Gattesco, N.; Oliveira, D.V. Experimental tests for the characterization of sisal fiber reinforced cementitious matrix for strengthening masonry structures. *Constr. Build. Mater.* **2019**, *219*, 44–55. [CrossRef]
30. Romanazzi, A.; Oliveira, D.V.; Silva, R.A. Experimental Investigation on the Bond Behavior of a Compatible TRM-based Solution for Rammed Earth Heritage. *Int. J. Archit. Herit.* **2019**, *13*, 1042–1060. [CrossRef]
31. John, S.K.; Nadir, Y.; Girija, K.; Giriprasad, S. Tensile behaviour of glass fibre textile reinforced mortar with fine aggregate partially replaced by fly ash. *Mater. Today Proc.* **2019**. [CrossRef]
32. Del Zoppo, M.; Di Ludovico, M.; Prota, A. Analysis of FRCM and CRM parameters for the in-plane shear strengthening of different URM types. *Compos. Part B Eng.* **2019**, *171*, 20–33. [CrossRef]
33. Del Zoppo, M.; Di Ludovico, M.; Balsamo, A.; Prota, A. In-plane shear capacity of tuff masonry walls with traditional and innovative Composite Reinforced Mortars (CRM). *Constr. Build. Mater.* **2019**, *210*, 289–300. [CrossRef]
34. Micelli, F.; Sciolti, M.S.; Leone, M.; Aiello, M.A.; Dudine, A. Shear behaviour of Fiber Reinforced Mortar strengthened masonry walls built with limestone blocks and hydraulic mortar. In *Brick and Block Masonry—Trends, Innovations and Challenges*; Modena, C., da Porto, F., Valluzzi, M.R., Eds.; Routledge: London, UK, 2016.
35. Gattesco, N.; Boem, I.; Andretta, V. Experimental behaviour of non-structural masonry vaults reinforced through fibre-reinforced mortar coating and subjected to cyclic horizontal loads. *Eng. Struct.* **2018**, *172*, 419–431. [CrossRef]
36. De Santis, S.; de Felice, G.; Di Noia, G.L.; Meriggi, P.; Volpe, M. Shake Table Tests on a Masonry Structure Retrofitted with Composite Reinforced Mortar. *Key Eng. Mater.* **2019**, *817*, 342–349. [CrossRef]
37. Abu-Jdayil, B.; Mourad, A.H.; Hittini, W.; Hassan, M.; Hameedi, S. Traditional, state-of-the-art and renewable thermal building insulation materials: An overview. *Constr. Build. Mater.* **2019**, *214*, 709–735. [CrossRef]
38. Longo, F.; Cascardi, A.; Lassandro, P.; Sannino, A.; Aiello, M.A. Mechanical and Thermal Characterization of FRCM-Matrices. *Key Eng. Mater.* **2019**, *817*, 189–194. [CrossRef]
39. Haq, E.U.; Padmanabhan, S.K.; Licciulli, A. In-situ carbonation of alkali activated fly ash geopolymer. *Constr. Build. Mater.* **2014**, *66*, 781–786. [CrossRef]
40. Provis, J.L.; Van Deventer, J.S.J. (Eds.) *Geopolymers: Structures, Processing, Properties and Industrial Applications*; Elsevier: New York, NY, USA, 2009.
41. Alanazi, H.; Hu, J.; Kim, Y.R. Effect of slag, silica fume, and metakaolin on properties and performance of alkali-activated fly ash cured at ambient temperature. *Constr. Build. Mater.* **2019**, *197*, 747–756. [CrossRef]
42. Longo, F.; Lassandro, P.; Moshiri, A.; Phatak, T.; Aiello, M.A.; Krakowiak, K.J. Lightweight geopolymer-based mortars for the structural and energy retrofit of buildings. *Energy Build.* **2020**, in press. [CrossRef]
43. Consiglio Superiore dei Lavori Pubblici. Linea Guida per la Identificazione, la Qualificazione ed il Controllo di Accettazione di Compositi Fibrorinforzati a Matrice Inorganica (FRCM) da Utilizzarsi per il Consolidamento Strutturale di Costruzioni Esistenti. In *Italian Standard for the Qualification of FRP Composites for the Externally Bonded Reinforcement of Existing Structures*; Consiglio Superiore dei Lavori Pubblici: Ravenna, Italy, 2015.
44. ASTM D7984-16. *Standard Test Method for Measurement of Thermal Effusivity of Fabrics Using a Modified Transient Plane Source (MTPS) Instrument*; ASTM International: West Conshohocken, PA, USA, 2016. Available online: www.astm.org (accessed on 30 July 2020).
45. UNI—Italian Organization for Standardization. *Methods of Test for Mortar for Masonry—Part 11: Determination of Flexural and Compressive Strength of Hardened Mortar*; EN 1015-11; UNI—Italian Organization for Standardization: Milano, Italy, 2007.
46. Scanning Electron Microscopy Specifications. Available online: https://www.zeiss.com/corporate/int/home.html?vaURL=www.zeiss.de/en (accessed on 30 June 2020).
47. Cheng, C.; He, J.; Zhang, J.; Yang, Y. Study on the time-dependent mechanical properties of glass fiber reinforced cement (GRC) with fly ash or slag. *Constr. Build. Mater.* **2019**, *217*, 128–136. [CrossRef]
48. Ministero delle Infrastrutture e dei Trasporti. *CNTC19-Circolare Applicativa delle Norme Tecniche delle Costruzioni di cui al DM 17 January 2018. (NTC 2018)*; Ministero delle Infrastrutture e dei Trasporti: Rome, Italy, 2019.

49.   UNI—Italian Organization for Standardization. *Thermal Performance of Building Components—Dynamic Thermal Characteristics-Calculation Methods*; EN ISO 13786:2008; UNI—Italian Organization for Standardization: Milano, Italy, 2008.

50.   UNI—Italian Organization for Standardization. *Masonry and Masonry Products—Methods for Determining Thermal Properties*; EN 1745:2012; UNI—Italian Organization for Standardization: Milano, Italy, 2012.

51.   Ozkahraman, H.T.; Bolatturk, A. The use of tuff stone cladding in buildings for energy conservation. *Constr. Build. Mater.* **2006**, *20*, 435–440. [CrossRef]

52.   Xie, C. Interactive Heat Transfer Simulations for Everyone. *Phys. Teach.* **2012**, *50*, 237–240. [CrossRef]

53.   De Santis, S.; de Felice, G.; Roscini, F. Retrofitting of Masonry Vaults by Basalt Textile-Reinforced Mortar Overlays. *Int. J. Archit. Herit.* **2019**, *13*, 1061–1077. [CrossRef]